R-matrix approach to collision processes: Study of the threshold behavior of $\gamma + \mathrm{He} \rightarrow \mathrm{He}^+(2s) + e^-$ or $\mathrm{He}^+(2p) + e^-$

Hao Xu and Robin Shakeshaft*

Physics Department, University of Southern California, Los Angeles, California 90089-0484, USA

(Received 14 September 2010; published 31 January 2011)

We report on a study of one-photon single ionization of $\mathrm{He}(1s^2)$ accompanied by excitation to $\mathrm{He}^+(2s)$ or $\mathrm{He}^+(2p)$ for photon energies at, and up to a few eV above, the excitation threshold. We find, both numerically and analytically, that as the photon energy approaches threshold from above the photoionization cross section turns sharply at about 200 meV and has a *cusp* at threshold. The cusp is associated with the adiabatic transfer of population between the $2s$ and $2p$ bound states of the ion. The photoelectron's electric field induces an energy splitting between the otherwise degenerate $2s$ and $2p$ states, and consequently the $2s$ and $2p$ populations oscillate with a period defined by this energy splitting. The number of oscillations is almost independent of the photoelectron's asymptotic speed v since over most of its outward journey the photoelectron moves with a speed much larger than v. However, on the last leg of its journey, after it has slowed down sufficiently in the Coulomb field of the ion, the photoelectron does move with an almost constant speed v. On this last leg the energy splitting is so small that there is insufficient time for $2s$ and $2p$ populations to undergo a full oscillation; rather, the (equal and opposite) changes in the $2s$ and $2p$ populations are proportional to v (i.e., to the square root of the excess photoelectron energy, which gives rise to a cusp).

DOI: 10.1103/PhysRevA.83.012716 PACS number(s): 03.65.Nk

I. INTRODUCTION

Almost 50 years ago Gailitis and Damburg showed that the cross section for an electron to scatter from a hydrogen atom at impact energies just above the $\mathrm{H}(n = 2)$ excitation threshold does not obey the normal Wigner threshold law, but instead depends on the logarithm of the excess energy, and in a way that is sinusoidal [1]. Similar behavior should be seen, in principle, in one-photon detachment of the negative hydrogen ion H^- at photoelectron energies just above the $\mathrm{H}(n = 2)$ threshold, but in practice is obscured by a ${}^1P^{\mathrm{o}}$ shape resonance. Cognizant of this, Liu *et al.* pointed out that since the shape resonance cannot be accessed by two photons, two-photon detachment of H^- should provide an unobstructed view of the anomalous threshold behavior [2]. They carried out detailed calculations, and found that the cross section for two-photon detachment of H^- to the $(n = 2)^1D^{\mathrm{e}}$ subchannel, when plotted versus the logarithm of the excess photoelectron energy, has a half-oscillation with large amplitude over the photoelectron energy range 0.5–34 meV above the $\mathrm{H}(n = 2)$ threshold [2].

In this paper we consider the threshold behavior of the cross section for one-photon ionization of helium accompanied by excitation to $\mathrm{He}^+(n = 2)$. The primary difference between photodetachment of H^- and photoionization of He is that in the latter process the photoelectron experiences a long-range Coulomb potential. We find that the cross section does not oscillate near threshold; rather, it exhibits a cusp. We present results of numerical calculations of the cross section for one-photon single ionization of $\mathrm{He}(1s^2)$ accompanied by excitation to $\mathrm{He}^+(2s/2p)$ for photoelectron energies near to, and up to roughly 7 eV above, the excitation threshold.

The origin of both the oscillatory behavior and the cusp is the long-range dipole interaction between the departing electron and the excited hydrogenic core which is in a superposition of $2s$ and $2p$ states. Due to the degeneracy of the $2s$ and $2p$ states the core has a permanent dipole moment $\vec{d}$ whose strength $|\vec{d}|$ (within zeroth-order perturbation theory) is a property of the core, but this dipole has an orientation which is either parallel, antiparallel, or perpendicular to the direction of motion of the unbound electron. If m and $-e$ denote the electron mass and charge, with $a_0 \equiv \hbar^2/me^2$ the Bohr radius, $|\vec{d}|$ is proportional to ea_0 with a constant of proportionality that is dimensionless and inversely proportional to the atomic number of the nucleus. In the field of the dipole the unbound electron experiences a potential which, up to a dimensionless constant that is independent of the electron charge, has the form $\hbar^2/(mr^2)$ at a distance $r \gg a_0$ from the core. In turn, the electric field of the unbound electron induces an energy splitting between the $2s$ and $2p$ states of the core. The interaction between the unbound electron and the core is attractive or repulsive, respectively, according to whether the dipole is parallel or antiparallel to the direction of motion of the outgoing electron. In general, the net dipole of the hydrogenic core is a superposition of parallel, antiparallel, and perpendicular dipoles. If the unbound electron moves slowly, the net dipole oscillates on the time scale defined by the energy splitting between the $2s$ and $2p$ states, and population is adiabatically transferred back and forth between the $2s$ and $2p$ states.

We digress for a moment to recall in more generality how a final-state interaction influences a transition rate. Suppose that a system undergoes a transition, due perhaps to a collision or half collision, and that one of the products is a particle which departs with energy $mv^2/2$ in an attractive potential that falls off slowly with distance r. We suppose that the asymptotic speed v is small. It is known from the theory of final-state interactions that the transition rate is enhanced by the long-range attractive tail of the potential since the unbound particle is delayed and spends more time in the region near the origin

*robins@usc.edu

where a transition is most likely to occur [3]. The effect appears as an enhancement of the particle's wave function at small r by a factor that is just the inverse of the Jost function [4]. When v is small the Jost function depends on v in roughly the same way as does the tangent of the phase shift. If, in addition, the potential does not fall off more rapidly with distance than $1/r^{2l+3}$, where l is the particle's orbital angular momentum quantum number, both the Jost function and the enhancement factor depend strongly on v.

Returning to our two-electron ion or atom, whose core is in a superposition of $2s$ and $2p$ states, let us focus first on the H^- system. Since the core is neutral the dominant potential experienced by the unbound electron in the final state is the $1/r^2$ potential. Assume that this potential is more attractive than the centrifugal barrier is repulsive. The unbound electron would spiral into the origin if the $1/r^2$ potential were to extend all the way to the origin. This fate is avoided by smoothly joining the $1/r^2$ potential at some small distance r_0 to a potential that is constant in the region $0 \leqslant r \leqslant r_0$ [5]. Now, rather than spiral into the origin, the unbound electron orbits the core a number of times and therefore experiences a significant delay before escaping. On dimensional grounds, since the only variables that enter the motion are $\hbar$, m, and the asymptotic speed v, the time delay must be $(\hbar/mv^2)$ up to a constant overall factor that depends on r_0/a_0. Recalling that the time delay is the derivative of the phase shift with respect to energy, we infer that the phase shift varies as $\ln v$, so the enhancement factor varies roughly as a cotangent whose argument depends on $\ln v$. It follows that the cross section has an oscillatory $\ln v$ dependence, in accord with the prediction of Gailitis and Damburg.

Once the unbound electron is further than a few a_0 or more from the hydrogenic core, the potential is relatively weak and the electron moves at a speed which does not differ greatly from its asymptotic speed v. Along the unbound electron's outward journey the $2s$ and $2p$ populations oscillate many times if v is small—*infinitely* many times in the adiabatic limit $v \to 0$. Thus in the adiabatic limit the $2s$ and $2p$ populations equalize at asymptotically large distances.

On the other hand, if, as we now suppose, the hydrogenic core has a net positive charge the attractive Coulomb interaction governs the motion of the unbound electron at large distances. We discuss this case in more detail in Sec. III. Briefly, while the asymptotic speed v may be small, along most of its outward journey the unbound electron moves with a speed much larger than v. Thus the $2s$ and $2p$ populations undergo only a relatively small number of oscillations. Only after the unbound electron has slowed down sufficiently in the Coulomb field of the ion, after a time $t \gtrsim (e^2/mv^3)$, does it move at a speed close to v. On this last leg of the journey, the energy splitting is so small that there is insufficient time for the $2s$ and $2p$ populations to undergo a full oscillation; rather, the changes in the $2s$ and $2p$ populations are proportional to v (i.e., to the square root of the excess energy of the unbound electron). Since the cross section is finite (nonzero) at the threshold $v = 0$ (the enhancement factor is infinite), it has a cusp.

Our calculations were performed using an R-matrix approach that accommodates the proper boundary conditions. This method has been described in detail elsewhere [6], and is sketched only briefly in the next section. In Sec. III we discuss the threshold behavior and the origin of the cusp; we give both mathematical and heuristic derivations of the threshold behavior. In Sec. IV we present our numerical results, which cover a range of photoelectron energies that extends from the $n = 2$ excitation threshold to the first Feshbach resonance below the $n = 3$ excitation threshold.

Although we consider, in this paper, energies at which only the $1s$, $2s$, and $2p$ subchannels are open, we take a moment to draw attention to the work of Hahn and Temkin who investigated two-electron escape by analytic continuation from below to above the total breakup threshold [7]. They developed a model where the outer electron moves, to a first approximation, in a potential that is Coulombic up to a certain distance, and of dipole form thereafter. Using the zero-energy solutions to this model, in combination with the optical potential, they derived various threshold laws for electron-impact ionization of hydrogen at different levels of approximation. A feature of special interest is the presence of repulsive terms in the optical potential at energies where more than a few subchannels are open; such terms inhibit two-electron escape.

II. METHOD

The system of interest is composed of an electron and a He^+ ion. Initially, this system is in its ground state. A photon is absorbed, and the system undergoes ionization. In the final state the system has a total energy E, one electron is free, the other is bound to the nucleus in the $1s$, $2s$, or $2p$ state. Our focus in this section is on the final state. We want to obtain the wave function for an electron that is incident on a He^+ ion in the $1s$, $2s$, or $2p$ state. The time-reversed wave function is needed to evaluate the transition amplitude for photoionization.

We partition the full state space into P and Q subspaces [8,9]. Four subchannels, the $1s\epsilon p$,$2s\epsilon p$,$2p\epsilon s$, and $2p\epsilon d$ subchannels, are included in P space. The remaining subchannels are relegated to Q space. Let $\mathbf{P}$ and $\mathbf{Q}$ be the operators which project onto the P and Q spaces. These spaces are coupled by the optical potential,

$$\mathbf{V}_{\rm opt}(E) \equiv \mathbf{PHQG}_Q(E)\mathbf{QHP}, \tag{1}$$

where $\mathbf{H}$ is the true Hamiltonian and $\mathbf{G}_Q(E)$ is the Q-space resolvent [i.e., $\mathbf{G}_Q(E) = \mathbf{Q}/(E\mathbf{1} - \mathbf{QHQ})$]. In the calculations reported on here, the photon energy lies below the threshold for excitation of $H(n = 3)$ so all subchannels in Q space are closed, and $\mathbf{G}_Q(E)$ can be replaced by its spectral decomposition. Let $|\Psi^{(i)}(E)\rangle$ represent the state of the system when the unbound electron is incident in the subchannel i, where $i(=1-4)$ denotes one of the subchannels belonging to P space. The projection $\mathbf{P}|\Psi^{(i)}(E)\rangle$ is a solution of the homogeneous equation,

$$[\mathbf{H}_{\rm eff}(E) - E\mathbf{1}]\mathbf{P}|\Psi\rangle = 0, \tag{2}$$

where $\mathbf{H}_{\rm eff}(E)$ is the energy-dependent effective Hamiltonian,

$$\mathbf{H}_{\rm eff}(E) = \mathbf{PHP} + \mathbf{V}_{\rm opt}(E). \tag{3}$$

The projection $\mathbf{Q}|\Psi^{(i)}(E)\rangle$ is $\mathbf{G}_Q(E)\mathbf{QHP}|\Psi^{(i)}(E)\rangle$, and this can be obtained once Eq. (2) has been solved, assuming that $\mathbf{G}_Q(E)$ is known.

The P-space wave function has the form (which must be symmetrized with respect to the electrons),

$$\frac{1}{r_1 r_2}\sum_j F_j^{(i)}(r_2)\phi_j(r_1,\hat{r}_1,\hat{r}_2) = \frac{1}{r_1 r_2}[\vec{F}^{(i)}(r_2)]^{\mathrm{t}}\vec{\phi}(r_1,\hat{r}_1,\hat{r}_2), \tag{4}$$

everywhere in position space. The "channel function" $F_j^{(i)}(r_2)$ is the radial wave function of the unbound electron, 2, in the entrance subchannel i, t denotes transpose, and $\phi_j(r_1,\hat{r}_1,\hat{r}_2)$ is the orthonormal wave function of the bound electron, 1, in state j. Thus the superscript i and the subscript j, respectively, on $F_j^{(i)}(r_2)$ denote the solution (the entrance subchannel) and the component of this solution on the channel basis; the sum on the right side of Eq. (4) is over all subchannels belonging to P space. We have incorporated the coupling of the angular momentum of the two electrons in $\phi_j(r_1,\hat{r}_1,\hat{r}_2)$. The general solutions of Eq. (2) are the elements of a four-dimensional column vector $\underline{F}^{\mathrm{t}}(r_2)\vec{\phi}(r_1,\hat{r}_1,\hat{r}_2)$, where $\underline{F}(r_2)$, the "channel matrix," is the matrix whose columns are the vectors $\vec{F}^{(i)}(r_2)$. To take into account the out-of-phase oscillations of incident and scattered waves we decompose the channel matrix into the sum of its "incident'—and "scattered"—wave components, that is, we write

$$\underline{F}(r) = \underline{F}_{\mathrm{scat}}(r) + \underline{F}_{\mathrm{inc}}(r). \tag{5}$$

The scattered-wave component $\underline{F}_{\mathrm{scat}}(r)$ is represented on a discrete basis that covers the volume of a "box" whose linear dimension is R. The incident-wave component $\underline{F}_{\mathrm{inc}}(r)$ is completely specified up to a normalization matrix $\underline{N}$ which is to be determined by matching $\underline{F}(r)$ and its derivative at the boundary $r = R$ to the exact solution of the Schrödinger equation for an unbound particle moving in the local potential due to the sum of Coulomb and static dipole fields.

The incident-wave component has the form $\underline{F}^{\mathrm{t}}_{\mathrm{inc}}(r) = \underline{N}^{\mathrm{t}}\,\underline{\mathcal{F}}^{\mathrm{t}}_{\mathrm{inc}}(r)$ where $\underline{\mathcal{F}}_{\mathrm{inc}}(r)$ is a diagonal matrix whose diagonal elements are

$$\mathcal{F}_{i,\mathrm{inc}}(r) = \hat{j}_{l_i}\left(k_i r + \gamma_i \ln\left(1+\frac{2k_i r}{c_i}\right) + \frac{\delta_i(k_i) r}{b_i + r}\right). \tag{6}$$

Here $\hat{j}_l(x)$ is a Riccati-Bessel function, $\hbar k_i$ and $\hbar l_i$ are the asymptotic linear and angular momenta of the unbound particle, $\gamma_i = Z'/(a_0 k_i)$ with $Z' = 1$ (the atomic number of the screened nucleus), b_i and c_i are positive parameters whose values are to be fixed, and $\delta_i(k_i)$ is a real variational parameter. The functions $\mathcal{F}_{i,\mathrm{inc}}(r)$ are regular at the origin and have the correct asymptotic forms. The logarithmic term $\ln[1+(2k_i r/c_i)]$ accounts for Coulomb distortion at large distances (i.e., distances where $k^2 r a_0 \gtrsim 1$). Since $\underline{F}(r)$ is to be matched to the asymptotic solution at $r = R$ we can restrict r to the range $r \leqslant R$. The logarithmic term is unwarranted if $k^2 R a_0 \lesssim 1$; hence c_i serves as a cutoff parameter, which we choose to be $c_i = 1 + (1/k_i^2 R a_0)$. The parameter b_i characterizes the radius of the core in the entrance subchannel i, and we fix its value to be 4 a.u. in all subchannels. Evidently, $\delta_i(k_i)$ is a phase shift. Its "optimal" value can be obtained from the Kohn variational principle, but we find that sufficient accuracy is obtained by fixing $\delta_i(k_i)$ to have the smallest absolute value for which $\mathcal{F}_{i,\mathrm{inc}}(R) \approx 1$, which is accomplished by taking

$$\delta_i(k_i) \approx -k_i R + l_i\frac{\pi}{2} - \gamma_i \ln\left(1+\frac{2k_i R}{c_i}\right) + (2n+1)\frac{\pi}{2}, \tag{7}$$

where the integer n is chosen so that $-\pi/2 < \delta_i(k_i) \leqslant \pi/2$.

The incident-wave component provides the source term in a linear inhomogeneous matrix equation for the scattered-wave component of the P-space wave function. This equation follows from substituting $\underline{F}(r) = \underline{F}_{\mathrm{scat}}(r) + \underline{F}_{\mathrm{inc}}(r)$ for $\mathbf{P}|\Psi\rangle$ in Eq. (2). We solve this equation by expanding $\underline{F}_{\mathrm{scat}}(r)$ on a hybrid basis whose radial functions are of the two types,

$$u_{nl}(r) = \frac{1}{\sqrt{R}}\hat{j}_l(k_n r), \quad k_n = \alpha_n/R, \quad n = 1,2,3,\ldots, \tag{8}$$

$$v_{nl}(r) = \sqrt{\frac{\kappa}{n(n-l)_{2l+1}}}(2\kappa r)^{l+1} L^{2l+1}_{n-l-1}(2\kappa r)e^{-\kappa r}, \quad n - l \ll \kappa R, \tag{9}$$

where α_n is the nth root of $\hat{j}_l(x)$ and $L^{\mu}_{\nu}(x)$ is an associated Laguerre polynomial. Both $u_{nl}(r)$ and $v_{nl}(r)$ vanish at the endpoints $r = 0$ and $r = R$ [or, more exactly, $v_{nl}(R)$ is exponentially small provided that the inverse-length-scale κ satisfies $n - l \ll \kappa R$]. Hence $\underline{F}_{\mathrm{scat}}(r)$ satisfies standing-wave boundary conditions [i.e., $\underline{F}_{\mathrm{scat}}(0) = 0 = \underline{F}_{\mathrm{scat}}(R)$].

In the region exterior to the box we attach a subscript to $\underline{F}(r)$ and its elements to indicate the type of asymptotic boundary condition that the solutions satisfy. The customary K-matrix asymptotic boundary conditions satisfied by the elements of the channel matrix are, for $r \gg R$,

$$F^{(i)}_{K_j}(r) \to \frac{1}{\sqrt{2\pi k_j}}\left[\sin\left(k_j r - \frac{1}{2}l_j\pi + \gamma_j \ln 2k_j r + \sigma_{l_j}\right)\delta_{ji} + \cos\left(k_j r - \frac{1}{2}l_j\pi + \gamma_j \ln 2k_j r + \sigma_{l_j}\right)K_{ji}\right], \tag{10}$$

where $\sigma_{l_j}(k_j)$ is the Coulomb phase shift (which we abbreviate to σ_{l_j}). However, since orbital angular momentum is exchanged over very large distances due to static dipole coupling, more suitable asymptotic boundary conditions with no dependence on angular momentum are ($r \gg R$)

$$F^{(i)}_{\tilde{K}j}(r) \to \frac{1}{\sqrt{2\pi k_j}}[\sin(k_j r + \gamma_j \ln 2k_j r + \sigma_0)\delta_{ji} + \cos(k_j r + \gamma_j \ln 2k_j r + \sigma_0)\tilde{K}_{ji}]. \tag{11}$$

We include the s-wave Coulomb phase shift σ_0 in all subchannels since this accounts for most of the Coulomb scattering at large distances, particularly near threshold; its presence ensures smooth threshold behavior. Following Seaton [10] we write

$$\underline{F}_{\tilde{K}}(r \geqslant R) = \underline{F}_{\sin}(r) + \underline{F}_{\cos}(r)\underline{\tilde{K}}, \tag{12}$$

where the matrices $\underline{F}_{\sin}(r)$ and $\underline{F}_{\cos}(r)$ are, for all $r \geqslant R$,

$$\underline{F}_{\sin}(r) = \underline{X}\,\underline{G}_{\sin}(r)\underline{X}^{\dagger}, \tag{13}$$

$$\underline{F}_{\cos}(r) = \underline{X}\,\underline{G}_{\cos}(r)\underline{X}^{\dagger}. \tag{14}$$

Here $\underline{X}$ is the constant, energy-independent, unitary matrix that diagonalizes the Hermitian matrix $-Z'e^2\underline{1}/r + (\hbar^2/2)\underline{A}/r^2$ where $\underline{A}$ includes both the angular momentum $\hbar^2 l(l+1)$ of the unbound electron and the static dipole of the residual ion that results from the coupling of degenerate eigenstates. We denote a generic eigenvalue of $\underline{A}$ by $\mu(\mu+1)$; thus μ is a generalized orbital angular momentum quantum number of the unbound electron. The matrices $\underline{G}_{\sin}(r)$ and $\underline{G}_{\cos}(r)$ are real and diagonal, and up to an overall factor of $1/\sqrt{2\pi k_i}$ and a sine and cosine, respectively, they approach the identity matrix at large r; at finite r their diagonal elements are

$$G_{\mu,\sin}(r) = (2\pi k_i)^{-1/2}\left[\sin\left(\mu\frac{\pi}{2} - \tilde{\sigma}_\mu\right) I_\mu(r) + \cos\left(\mu\frac{\pi}{2} - \tilde{\sigma}_\mu\right) R_\mu(r)\right], \tag{15}$$

$$G_{\mu,\cos}(r) = (2\pi k_i)^{-1/2}\left[\cos\left(\mu\frac{\pi}{2} - \tilde{\sigma}_\mu\right) I_\mu(r) - \sin\left(\mu\frac{\pi}{2} - \tilde{\sigma}_\mu\right) R_\mu(r)\right], \tag{16}$$

where

$$\tilde{\sigma}_\mu = \sigma_\mu - \sigma_0, \tag{17}$$

and where σ_μ is the generalized Coulomb phase shift, defined for real and complex μ as

$$\sigma_\mu = -\frac{i}{2}\ln\left(\frac{\Gamma(\mu+1-i\gamma_j)}{\Gamma(\mu+1+i\gamma_j)}\right), \tag{18}$$

and where $R_\mu(r)$ and $I_\mu(r)$, respectively, are the regular and irregular Coulomb wave functions (normalized asymptotically to a sin and cosine with unit amplitude) with μ replacing the conventional orbital angular momentum quantum number. Thus an arbitrary component of Eq. (13) is

$$F^{(i)}_{j,\sin}(r) = \sum_\mu X_{j\mu} G_{\mu,\sin}(r) X^*_{i\mu}. \tag{19}$$

(Complex conjugation of $\underline{X}$ is unnecessary if, as in the present case, $\underline{X}$ is real.) If $r \gg R$ the matrices $\underline{F}_{\sin}(r)$ and $\underline{F}_{\cos}(r)$ are diagonal, and the asymptotic form on the right side of Eq. (11) follows from Eqs. (12)–(14).

Each eigenvalue a of $\underline{A}$ is real, and is related to μ by $\mu = -\frac{1}{2} + \sqrt{a+\frac{1}{4}}$. Hence μ is complex if $a < -\frac{1}{4}$, in which case its real part is $-\frac{1}{2}$. When $a < -\frac{1}{4}$ the repulsive semiclassical angular momentum barrier $(l+\frac{1}{2})^2(\hbar^2/2r^2)$ is overwhelmed by the attractive dipole potential. In general, the potential experienced by the unbound electron due to the dipole field of the ion is attractive, repulsive, or zero, respectively, according to whether the residual ion's dipole is parallel, antiparallel, or orthogonal to the direction of motion of the unbound electron. However, the orientation of the dipole is sharply defined only for certain linear combinations of the degenerate eigenstates of the residual ion. When both the total orbital angular momentum of the two electrons, and the generalized orbital angular momentum quantum number μ of the unbound electron, are sharply defined, the orientation of the dipole is not sharply defined. Nevertheless, if the most likely value of the orbital angular momentum quantum number of the unbound electron is l we can say that among the three possible sharply defined orientations of the dipole the favored one is orthogonal, parallel, or antiparallel, respectively, if the eigenvalue a is comparable to, much less than, or much greater than $l(l+1)$.

In the present case the total orbital angular momentum quantum number of the two-electron system in its final state is 1, and since the residual ion is left in the $2s$ or $2p$ state the possible orbital angular momentum quantum numbers of the unbound electron are 0, 1, and 2. The possible generalized orbital angular momentum quantum numbers of the unbound electron are

$$\mu = \begin{cases} 1 & \rightleftarrows\ 2s\epsilon p \\ -\frac{1}{2} + \frac{i}{2}\sqrt{12(1+\zeta^2)^{1/2} - 13} & \rightleftarrows\ 2p\epsilon s \\ -\frac{1}{2} + \frac{1}{2}\sqrt{13 + 12(1+\zeta^2)^{1/2}} & \rightleftarrows\ 2p\epsilon d, \end{cases}$$

where ζ measures the strength of the dipole coupling of $2s$ or $2p$ bound states, and in the present case has the value $\zeta = 1$. The two-electron configuration to which each value of μ correlates in the limit of no dipole coupling (i.e., $\zeta = 0$) is shown to the right of the expression for μ. Evidently, it is the $2p\epsilon s$ configuration that is associated with the most strongly attractive dipole interaction, whereas the $2p\epsilon d$ configuration is associated with the most strongly repulsive interaction.

The scattering matrix $\underline{S}$ is related to the $\underline{\tilde{K}}$ matrix by

$$\underline{S} = \underline{D}\left(\frac{\underline{1} + i\underline{\tilde{K}}}{\underline{1} - i\underline{\tilde{K}}}\right)\underline{D}, \tag{20}$$

where $\underline{D}$ is a diagonal matrix whose diagonal elements are $e^{i(\frac{1}{2}l_j\pi - \tilde{\sigma}_{l_j})}$. Before calculating $\underline{S}$ we added to $\underline{\tilde{K}}$ the first-order correction which follows from the Kohn variational principle [6]. Thereby we improved the accuracy of $\underline{S}$.

III. THRESHOLD BEHAVIOR

A. Mathematical derivation

Suppose that in a particular subchannel the unbound electron has a momentum $\hbar k$ which is small. The s-wave Coulomb phase shift $\sigma_0(k)$ varies rapidly with k near the threshold $k = 0$, and diverges there as $-(Z'/a_0k)\ln k$. In contrast, $\tilde{\sigma}_\mu(k)$ varies smoothly:

$$\tilde{\sigma}_\mu(k) = -\mu\frac{\pi}{2}\coth\pi\gamma - \frac{1}{2\gamma} + O((\mu k a_0)^2), \tag{21}$$

with $\gamma = Z'/(a_0k)$. It follows from Eqs. (15) and (16) that if μ is an integer $G_{\mu,\sin}(r)$ and $G_{\mu,\cos}(r)$ develop into the regular and irregular Coulomb wave functions, $R_\mu(r)$ and $I_\mu(r)$, respectively, as a threshold is approached. If μ is not an integer $G_{\mu,\sin}(r)$ and $G_{\mu,\cos}(r)$ remain linear combinations of regular and irregular Coulomb wave functions even at threshold.

No matter whether or not μ is an integer, both $G_{\mu,\sin}(r)$ and $G_{\mu,\cos}(r)$ are independent of k for small k provided that

$$k^2 \ll Z'/(a_0 r). \tag{22}$$

To see this we first observe that if the preceding inequality is obeyed $R_\mu(r)$ can be expanded in terms of regular Bessel functions $J_{2\mu+1+m}(2\sqrt{2Z'r/a_0})$, and $I_\mu(r)$ can be expanded in terms of irregular Bessel functions $Y_{2\mu+1+m}(2\sqrt{2Z'r/a_0})$, where m is a non-negative integer [11]. Retaining only the first term in each series, we have the approximations,

$$R_\mu(r) \approx -\beta(\mu,k)\left(\frac{Z'r}{2a_0}\right)^{1/2} J_{2\mu+1}(2\sqrt{2Z'r/a_0}), \tag{23}$$

$$I_\mu(r) \approx -\frac{\pi}{\beta(\mu,k)}\left(\frac{Z'r}{2a_0}\right)^{1/2} Y_{2\mu+1}(2\sqrt{2Z'r/a_0}), \tag{24}$$

where

$$\beta(\mu,k) = e^{\frac{1}{2}\gamma\pi - i\sigma_\mu}\frac{\Gamma(\mu+1-i\gamma)}{\gamma^{\mu+1}}. \tag{25}$$

The relative correction is of order $(ka_0)(kR)$ for $r \leqslant R$. When μ is real, $\beta(\mu,k)$ is real and (recall Sterling's formula) is proportional to $\sqrt{k}$ with a relative correction of order $(\mu k a_0)^2$. Since the latter correction is analytic in μ we infer that $\beta(\mu,k)$ is also proportional to $\sqrt{k}$ when μ is complex. Therefore, $R_\mu(r)/\sqrt{2\pi k}$ and $I_\mu(r)/\sqrt{2\pi k}$ are independent of k for small k, with a relative correction of order $(ka_0)(kR)$. Combining this result with Eqs. (15), (16), and (21) it follows that both $G_{\mu,\sin}(r)$ and $G_{\mu,\cos}(r)$ are independent of k for both real and complex μ, with a relative correction of *first* order in k

From Eqs. (12)–(14) we see that the energy-normalized solution in the interior $r < R$ must fit smoothly to

$$\underline{X}\,\underline{G}_{\sin}(r)\underline{X}^\dagger + \underline{X}\,\underline{G}_{\cos}(r)\underline{X}^\dagger\underline{\tilde{K}}$$

at $r = R$. If inequality (22) holds, the solution in the interior is energy independent up to a correction of order $(ka_0)(kR)$, aside from a normalization factor. [Note that this inequality cannot be satisfied when $Z' = 0$; thus $Z = 1$ is a singularity.] Since $\underline{G}_{\sin}(r)$ is energy independent so, too, must be the normalization factor of the interior solution. Since $\underline{G}_{\cos}(r)$ is also energy independent, so, too, must be $\underline{\tilde{K}}$. If μ is real the leading correction to the zero-energy limit of $\underline{\tilde{K}}$ is of second order in k. On the other hand, if μ is complex the leading correction is of *first* order in k. The reason is as follows: Recall that $G_{\mu,\sin}(r)$ and $G_{\mu,\cos}(r)$ are each independent of k up to a correction of first order in k. However, the exterior solution matches smoothly at $r = R$ to an energy-independent solution in the interior region which is *regular* at the origin. Hence when $kR \ll 1$ the $\tilde{K}$ matrix must mix $G_{\mu,\sin}(R)$ and $G_{\mu,\cos}(R)$ so that their combination is the regular solution. If μ is real the regular solution is $R_\mu(R)$; thus, the correct combination is

$$\cos\left(\mu\frac{\pi}{2} - \tilde{\sigma}_\mu\right)G_{\mu,\sin}(r) + \sin\left(\mu\frac{\pi}{2} - \tilde{\sigma}_\mu\right)G_{\mu,\cos}(r) = \frac{1}{\sqrt{2\pi k}}R_\mu(r), \tag{26}$$

and since $R_\mu(R)/\sqrt{2\pi k}$ is energy independent up to a correction of second order in k, so too must be $\underline{\tilde{K}}$. In other words the terms that are linear in k are canceled when $G_{\mu,\sin}(R)$ and $G_{\mu,\cos}(R)$ are combined. However, if μ is complex $Y_{2\mu+1}(2\sqrt{2Z'r/a_0})$ and $J_{2\mu+1}(2\sqrt{2Z'r/a_0})$ are equally singular at $r = 0$, so both are acceptable. In this case it is the energy dependence of $G_{\mu,\sin}(R)$ and $G_{\mu,\cos}(R)$ that matters. Hence when μ is complex the $\tilde{K}$ matrix, and therefore the K matrix, are constant with a correction that is proportional to the square root of the excess photoelectron energy above threshold. Consequently, the K matrix, and therefore the cross section, have a cusp at threshold.

B. Heuristic derivation

Consider times $t \geqslant 0$ long after photoejection has occurred. Suppose that the photoelectron is at a distance $r(t)$ from the nucleus which is significantly larger than a_0, and that it is moving in a direction $\hat{r}$ that is almost constant. The zeroth-order perturbed states of the ion are the linear combinations $2s \pm 2p$ represented by

$$|\pm\rangle = \frac{1}{\sqrt{2}}(|2s\rangle \pm |2p\rangle). \tag{27}$$

Here we are interested only in the $2p$ state that is oriented along $\hat{r}$; we omit the orthogonal $2p$ state since it is not mixed with the $2s$ state by the photoelectron's electric field. In the state $+$ or $-$ the excited He^+ ion has a dipole $\pm d|e|a_0\hat{r}$ where $-e$ is the electron charge and where $d = |\langle 2p|z|2s\rangle|/a_0 = 3/Z$ with $Z = 2$.

Suppose that at time $t = 0$ the ion is in the state,

$$|\psi(0)\rangle = f_+(|2s\rangle + |2p\rangle) + f_-(|2s\rangle - |2p\rangle), \tag{28}$$

where $|f_+|^2 + |f_-|^2 = 1/2$. Without loss in generality we can choose f_+ and f_- to have equal but opposite phases, $\pm\phi/2$ say. The kets $|\pm\rangle$ do not depend on the strength of the interaction between the photoelectron and the ion and therefore do not depend on $r(t)$. Hence, as long as the "frequency" $(dr/dt)/a_0$ of the photoelectron's motion is small compared to the smallest frequency for a transition out of the $2s/2p$ manifold the state ket of the ion evolves adiabatically. Therefore, the state ket at times $t > 0$ is, up to an overall phase factor,

$$|\psi(t)\rangle = f_+(|2s\rangle + |2p\rangle) + f_- e^{-(i/\hbar)\int_0^t dt'\,\Delta E(t')}(|2s\rangle - |2p\rangle), \tag{29}$$

where $\Delta E(t)$ is the energy splitting of the $\pm$ levels at time t, that is,

$$\Delta E(t) = (3/Z)e^2 a_0/r^2(t). \tag{30}$$

The populations of the $2s$ and $2p$ states of the ion vary quasiperiodically in time with a period of order $\hbar/|\Delta E(t)|$, and at $t \sim \infty$ these populations are P_{2s} and P_{2p}, respectively, where

$$P_{2s} = |f_+ + f_-|^2 - 2|f_+ f_-|[\cos\phi + \cos(\phi + \Theta)], \tag{31}$$

$$P_{2p} = |f_+ + f_-|^2 - 2|f_+ f_-|[\cos\phi - \cos(\phi + \Theta)], \tag{32}$$

and where

$$\Theta = 3(e^2 a_0/Z\hbar)\int_0^\infty \frac{dt}{r^2(t)}. \tag{33}$$

It remains to determine $r(t)$.

If the asymptotic speed v of the photoelectron is small, the motion of the photoelectron is governed primarily by the Coulomb potential $-Z'e^2/r$ where $Z' = Z - 1$. Retaining only this potential, and neglecting the rotational energy which is small compared to the Coulomb energy at large distances, the classical equation for the radial motion of the photoelectron is, using conservation of energy,

$$m(dr/dt)^2/2 \approx mv^2/2 + Z'e^2/r. \tag{34}$$

If the Coulomb energy is much larger in magnitude than the total energy, that is, if

$$Z'e^2/r \gg mv^2/2, \tag{35}$$

we can drop the total energy in Eq. (34); the photoelectron's speed is

$$dr/dt \approx (Z'e^2/mr)^{1/2}, \tag{36}$$

and integrating this result gives

$$r(t) \approx (9Z'e^2/2m)^{1/3}t^{2/3} + \text{const.}. \tag{37}$$

The photoelectron does not move with constant speed v until near the end of its outward journey, at times when the Coulomb energy is much smaller in magnitude than the total energy. Thus, reversing inequality (35), and using Eq. (37) we see that the photoelectron moves with (almost) constant speed v when

$$t \gg Z'(e^2/mv^3). \tag{38}$$

Hence there are two distinct contributions to Θ [to the integral over t on the right side of Eq. (33)]. The first contribution comes from the range $0 \leqslant t \lesssim Z'(e^2/mv^3)$ where the Coulomb energy dominates, and where we can insert the right side of Eq. (37) for $r(t)$. This contribution is relatively insensitive to v; it is linear in v with a constant term that dominates. The second contribution comes from the range $t \gtrsim Z'(e^2/mv^3)$ where the photoelectron moves almost with constant speed v, and where we can insert $r(t) \approx vt$; this contribution is of order,

$$\frac{e^2a_0}{Z\hbar}\int_{Z'(e^2/mv^3)}^{\infty}\frac{dt}{(vt)^2} \sim \frac{1}{Z'Z}\left(\frac{\hbar v}{e^2}\right), \tag{39}$$

which yields small equal but opposite corrections to the $2s$ and $2p$ populations that are proportional to the square root of the excess photoelectron energy. Hence the partial cross sections for excitation to the $2s$ and $2p$ states exhibit cusps. In view of the fact that the $2p\epsilon d$ configuration is the most closely associated with a repulsive dipole interaction, we expect the $2p\epsilon s$ configuration to contribute more than the $2p\epsilon d$ configuration to the cusp.

C. Comparison with $\gamma + H^- \rightarrow H(2s/2p) + e^-$

We briefly comment on another process, photodetachment of H^- with excitation to $H(2s/2p)$. There are some interesting differences that arise because the photoelectron is screened from the nucleus by the bound electron (i.e., because $Z' = 0$). The photoelectron moves with a speed that is almost constant along its entire outward journey. Hence, at photon energies near threshold, where v is small, population is transferred back and forth between the $2s$ and $2p$ states many times—infinitely many times as $v \rightarrow 0$. Hence, in the adiabatic limit the hydrogen atom is left in an *equal* mixture of $2s$ and $2p$ states. We can see this by putting $Z' = 0$ and replacing Eq. (37) by

$$r^2(t) \approx a^2 + (vt)^2, \tag{40}$$

so now, with $Z = 1$, we have

$$\Theta \approx 3\pi(e^2a_0/2av\hbar). \tag{41}$$

Thus the small-v dependence of Θ changes from v to $1/v$ when $Z' = 0$. In the limit $v \rightarrow 0$ the term $\cos(\phi + \Theta)$ on the right sides of Eqs. (31) and (32) oscillates infinitely rapidly and averages to zero to give $P_{2s} = P_{2p} = |f_+|^2 + |f_-|^2 = 1/2$.

As noted in Sec. I, when the atom's dipole is parallel to the direction of motion of the outgoing photoelectron the cross section oscillates versus $\ln v$ near threshold. By contrast the cross section for photoionization of He with excitation to $He^+(2s/2p)$ does not oscillate near threshold. The dipole field is not important beyond a distance of about $(\hbar/mv)$, but the Coulomb field exerts the dominant influence on the photoelectron's radial motion well before this distance is reached. In fact, at the distance $(\hbar/mv)$ the Coulomb potential energy is $Z'e^2mv/\hbar$, which exceeds the photoelectron's energy if $Z'(e^2/\hbar v) \gtrsim 1$.

IV. RESULTS

Now we present results for one-photon single ionization of He accompanied by excitation to the $2s$ and $2p$ states of He^+, assuming the light is linearly polarized. Our calculations required only modest computer resources. We used a box radius of $R = 70$ a.u. and we employed independent-electron orbtial angular momentum quantum numbers ranging from 0 to 3. The scattered-wave component $\underline{F}_{\text{scat}}(r)$ of the P-space wave function was represented mostly by Riccati-Bessel functions, 50 for the $1s$ subchannel and 27 for the other subchannels, and only a few Sturmian functions, 10 for the $1s$ subchannel and 4 for the other subchannels. The wave numbers k_n—recall Eq. (8)—were chosen so that the energy of the photoelectron is closely surrounded by at least a few eigenvalues of **PHP**. The ground-state wave function was represented on a basis whose radial part was composed purely of Sturmian functions, 30 per electron per angular momentum quantum number. A similar basis was used to represent Q space, with either 15 or 30 Sturmian functions per electron per angular momentum quantum number. Generally, our estimates of the K matrix were symmetric to at least three significant figures before adding the variational correction, and to at least six significant figures after adding this correction. Typically, we found the average variational correction to be between 3% and 5% close to threshold (i.e., for photon energies below 66.7 eV), and less than 1% at higher energies. Results obtained in the velocity gauge differed from those in the length gauge by less than 0.01%.

We show results for photon energies from the $2s(2p)$ excitation threshold to about 7 eV above this threshold in Figs. 1–8. Where possible we compare our results with other

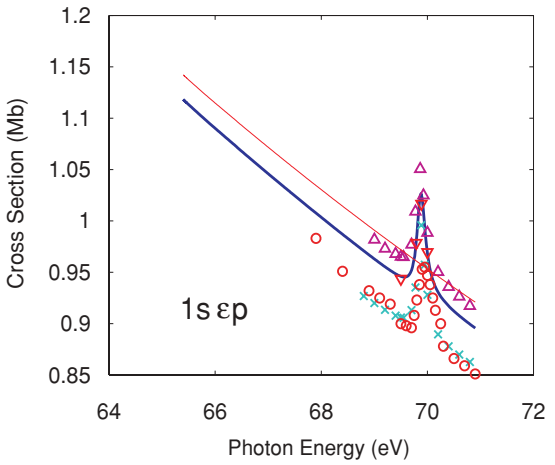

FIG. 1. (Color online) Partial cross section for one-photon ionization of He to the $1s\epsilon p$ subchannel. (Thick solid line) Present results, including optical potential. (Thin solid line) Present results, excluding optical potential. (Crosses) Sánchez and Martín [12]. (Triangles) Declever *et al.* [13]. (Inverted triangles) Jiang *et al.* [14]. (Circles) Experiment of Lindle *et al.* [15].

theoretical results and also with experimental data. In general, our results are in excellent agreement with those of Jiang *et al.* [14], they used the traditional *R*-matrix method. To assess the importance of the optical potential in the background region we show, in most of the figures, both results obtained from including and from excluding this potential. The optical potential accounts for closed-channel (Feshbach) resonances, and if it is omitted those resonances do not appear.

The partial cross section for photoionization without excitation is shown in Fig. 1. The main feature is the closed-channel resonance. Our results agree well with the shape of the experimental data from Lindle, but in absolute magnitude the latter lie about 5% below our results. At photon energies below

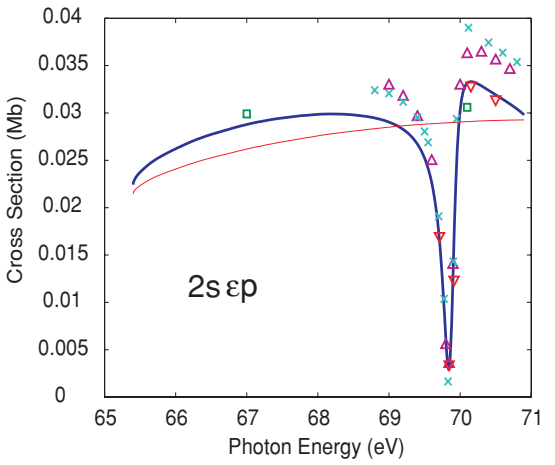

FIG. 2. (Color online) Partial cross section for one-photon ionization of He to the $2s\epsilon p$ subchannel. (Thick solid line) Present results, including optical potential. (Thin solid line) Present results, excluding optical potential. (Crosses) Sánchez and Martín [12]. (Triangles) Declever *et al.* [13]. (Inverted triangles) Jiang *et al.* [14]. (Squares) Experiment of Woodruff and Samson [16].

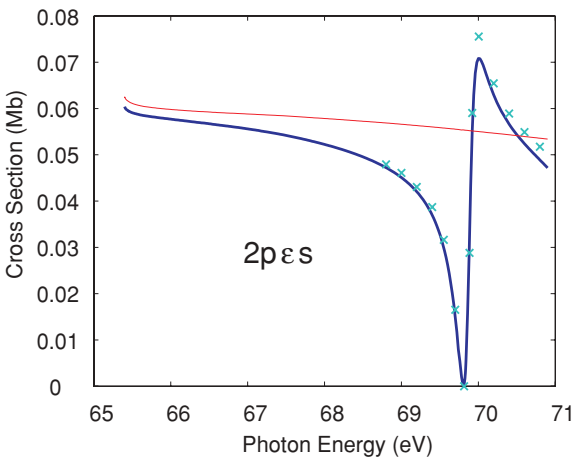

FIG. 3. (Color online) Partial cross section for one-photon ionization of He to the $2p\epsilon s$ subchannel. (Thick solid line) Present results, including optical potential. (Thin solid line) Present results, excluding optical potential. (Crosses) Sánchez and Martín [12].

about 69 eV the cross section follows an almost perfectly straight line all the way to the threshold.

In Fig. 2 the partial cross section for photoionization with excitation to the $2s\epsilon p$ subchannel is shown. There is reasonable agreement among the theoretical results, all of which nearly coincide with the single experimental data point on the resonance profile. There is one other experimental data point below the resonance region, which sits just above our curve. In this region we find that the cross section slopes gently downward as the photon energy decreases, but turns sharply downward just above threshold.

The partial cross section for photoionization with excitation to the $2p\epsilon s$ subchannel is shown in Fig. 3. We find that below the resonance region the cross section slopes gently upward as the photon energy decreases, but turns sharply upward just above threshold. In Fig. 4 the partial cross section for photoionization with excitation to the $2p\epsilon d$ subchannel is shown. In the region below the resonance we find that the

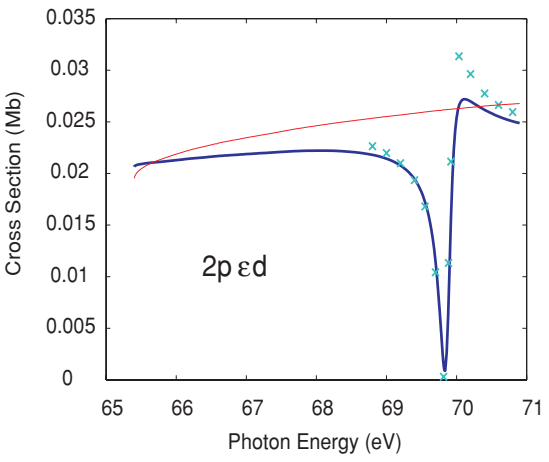

FIG. 4. (Color online) Partial cross section for one-photon ionization of He to the $2p\epsilon d$ subchannel. (Thick solid line) Present results, including optical potential. (Thin solid line) Present results, excluding optical potential. (Crosses) Sánchez and Martín [12].

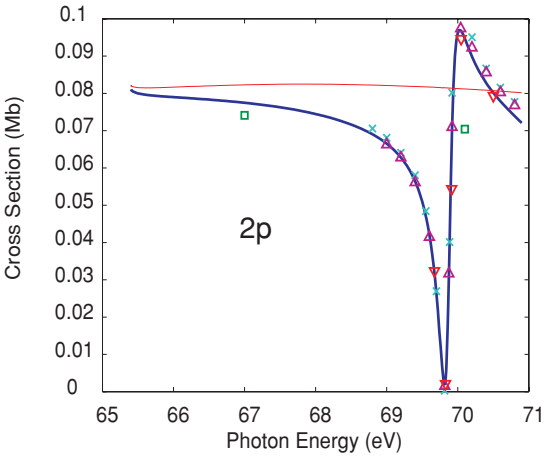

FIG. 5. (Color online) Partial cross section for one-photon ionization of He to the $2p$ state of He^+, summed over the $2p\epsilon s$ and $2p\epsilon d$ subchannels. (Thick solid line) Present results, including optical potential. (Thin solid line) Present results, excluding optical potential. (Crosses) Sánchez and Martín [12]. (Triangles) Declever *et al.* [13]. (Inverted triangles) Jiang *et al.* [14]. (Squares) Experiment of Woodruff and Samson [16].

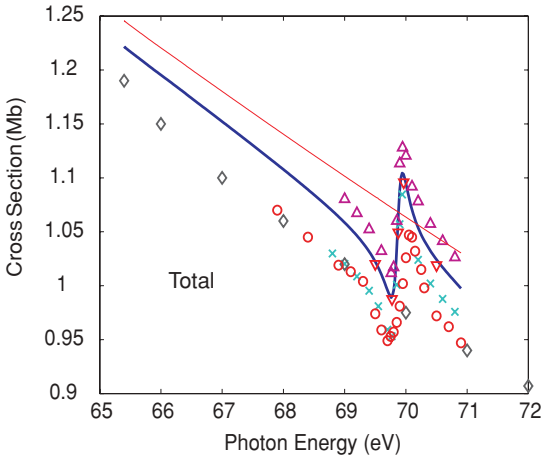

FIG. 7. (Color online) Total cross section for one-photon ionization of He, summed over all open subchannels ($1s\epsilon p$,$2s\epsilon p$,$2p\epsilon s$, and $2p\epsilon d$). (Thick solid line) Present results, including optical potential. (Thin solid line) Present results, excluding optical potential. (Crosses) Sánchez and Martín [12]. (Triangles) Declever *et al.* [13]. (Inverted triangles) Jiang *et al.* [14]. (Circles) Experiment of Lindle *et al.* [15]. (Diamonds) Experiment of Samson *et al.* [18].

cross section is almost flat, but that if the optical potential is omitted the cross section turns sharply downward just above threshold.

Evidently, the neglect of the optical potential can significantly affect the background cross section, particularly in the case of photoionization without excitation where it leads to an overestimate of the cross section. Various combinations of the partial cross sections are shown in Figs. 5–7 for the purpose of comparison with data available from experiments.

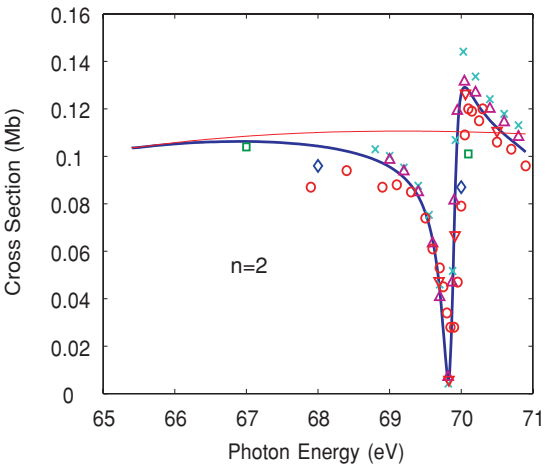

FIG. 6. (Color online) Partial cross section for one-photon ionization of He to the $n = 2$ level of He^+, summed over the $2s\epsilon p$, $2p\epsilon s$, and $2p\epsilon d$ subchannels. (Thick solid line) Present results, including optical potential. (Thin solid line) Present results, excluding optical potential. (Crosses) Sánchez and Martín [12]. (Triangles) Declever *et al.* [13]. (Inverted triangles) Jiang *et al.* [14]. (Circles) Experiment of Lindle *et al.* [15]. (Squares) Experiment of Woodruff and Samson [16]. (Diamonds) Experiment of Bizau and Wuilleumier [17].

In Fig. 8 we provide a detailed look at the partial cross sections close to threshold. The partial $2s\epsilon p$ and $2p\epsilon s$ cross sections exhibit a cusp at threshold while the partial $2p\epsilon d$ cross section is (almost) flat. Furthermore, the decrease in the partial $2s\epsilon p$ cross section near threshold is offset by an equal increase in the partial $2p\epsilon s$ cross section. Although the Lamb shift spoils the perfect degeneracy of the $2s$ and $2p$ states, this shift is only about 0.073 meV and therefore we would not expect it to significantly modify the results shown in Fig. 8. The cusp may be observable through a measurement of the ratio of the partial cross sections for either (i) $2s\epsilon p$ and $2p\epsilon d$ excitation, or (ii) $2p\epsilon s$ and $2p\epsilon d$ excitation, or (iii) $2s\epsilon p$ and $2p\epsilon s$ excitation, where the last ratio drops and then flattens out as threshold is approached.

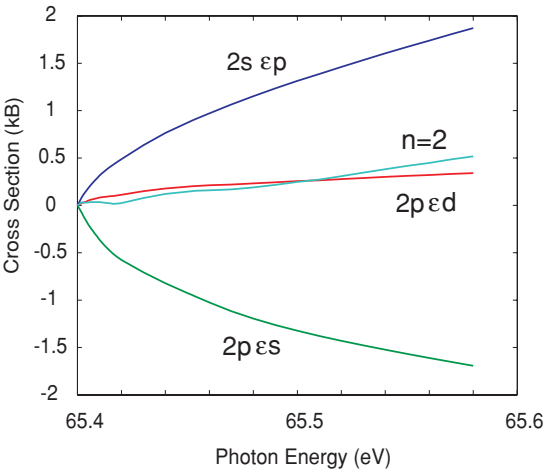

FIG. 8. (Color online) Partial cross sections for photoionization of He accompanied by excitation to $He^+(2s/2p)$ just above the excitation threshold. The partial cross sections have been shifted vertically so that they coincide at threshold.

[1] M. Gailitis and R. Damburg, Proc. Phys. Soc. **82**, 192 (1963).
[2] C.-R. Liu, N.-Y. Du, and A. F. Starace, Phys. Rev. A **43**, 5891 (1991).
[3] K. M. Watson, Phys. Rev. **88**, 1153 (1952).
[4] The Jost function is $(\hbar/mv)$ times the Wronskian of the regular and irregular wave functions of the particle, where the irregular wave function is normalized to an outgoing wave with unit amplitude at $r \sim \infty$, and the regular wave function is normalized to a free-particle wave function at $r \sim 0$, which in turn is normalized to a standing wave with unit amplitude at $r \sim \infty$.
[5] L. D. Landau and E. M. Lifshitz, *Quantum Mechanics*, 3rd ed. (Butterworth Heinemann, Oxford, 1999).
[6] H. Xu and R. Shakeshaft (unpublished).
[7] A. Temkin and Y. Hahn, Phys. Rev. A **9**, 708 (1974); A. Temkin, Phys. Rev. Lett. **49**, 365 (1982); Phys. Rev. A **30**, 2737 (1984).
[8] H. Feshbach, Ann. Phys. (NY) **5**, 357 (1958).
[9] Y. Hahn, T. F. O'Malley, and L. Spruch, Phys. Rev. **128**, 932 (1962).
[10] M. J. Seaton, Proc. Phys. Soc. **77**, 174 (1961).
[11] F. L. Yost, J. A. Wheeler, and G. Breit, Phys. Rev. **49**, 174 (1936).
[12] I. Sánchez and F. Martín, Phys. Rev. A **44**, 7318 (1991).
[13] P. Decleva, A. Lisini, and M. Venuti, J. Phys. B: At. Mol. Opt. Phys. **27**, 4867 (1994).
[14] Y. H. Jiang, R. Püttner, and G. Kaindl, J. Phys. B: At. Mol. Opt. Phys. **38**, 2157 (2005).
[15] D. W. Lindle, T. A. Ferrett, P. A. Heimann, and D. A. Shirley, Phys. Rev. A **36**, 2112 (1987).
[16] P. R. Woodruff and J. A. R. Samson, Phys. Rev. A **25**, 848 (1982).
[17] J. M. Bizau and F. J. Wuilleumier, J. Electron Spectrosc. Relat. Phenom. **71**, 205 (1995).
[18] J. A. R. Samson, Z. X. He, L. Yin, and G. N. Haddad, J. Phys. B: At. Mol. Opt. Phys. **27**, 887 (1994).